Supporting Information

Monolithic mesoporous graphitic composites as supercapacitors: from Starbons to Starenes®

*Andrea Muñoz García, Vitaliy L. Budarin, Yixin Zhou, Mario De bruyn, Andrew J. Hunt, Leonardo Lari, Vlado K. Lazarov, Horacio J. Salavagione, Enrique Morales, Gary J. Ellis, James H. Clark, Peter S. Shuttleworth**

Andrea Muñoz García, Yixin Zhou, Dr. Vitaliy L. Budarin, Dr. Mario De bruyn, Dr. Andrew J. Hunt, Prof. James H. Clark
Department of Chemistry, University of York, Heslington, York, YO10 5DD, UK,

Dr. Andrew J. Hunt
Khon Kaen University, Department of Chemistry, Faculty of Science, Khon Kaen University Khon Kaen, Khon Kaen, TH 40002

Dr. Leonardo Lari, Dr. Vlado Lazarov
York JEOL Nanocentre, Helix House, Science Park,
University of York, Heslington, York, YO10 5BR, UK

Dr. Enrique Morales, Dr. Horacio J. Salavagione, Dr. Gary J. Ellis, Dr. Peter S. Shuttleworth
Departamento de Física de Polímeros, Elastómeros y Aplicaciones Energéticas,
Instituto de Ciencia y Tecnología de Polímeros, CSIC, c/Juan de la Cierva, 3,
28006 Madrid, Spain
*E-mail: peter@ictp.csic.es

Experimental

Wide angle X-ray scattering (WAXS): A Bruker D8 Advance diffractometer was used to record the room temperature diffractograms at an intensity of 40 mA and voltage of 40 kV. Diffractograms were performed over the angular range of $2\theta = 10^{\circ} – 35^{\circ}$, with an accumulation time of 3s at each increment of 0.05º. Bragg's equation was used to calculate of the d-spacing: $n\lambda = 2d \sin \theta$, where λ is the wavelength of the X-ray, d is the interlayer distance and θ is the angle of incident X-ray radiation.

Measurements were undertaken in the Raman Microspectroscopy Laboratory of the Characterisation Service in the Institute of Polymer Science & Technology, CSIC using a Renishaw InVia-Reflex Raman system (Renishaw plc, Wotton-under-Edge, UK), which employed a grating spectrometer with a Peltier-cooled CCD detector coupled to a confocal microscope. The Raman scattering was excited with an argon ion laser (λ = 514.5 nm), focusing on the sample with a 100x microscope objective (NA=0.85) with a laser power of approximately 2 mW at the sample. Spectra were recorded in the range between 1000 and 3200 cm^{-1}. All spectral data was processed with Renishaw WiRE 3.3 software.

Results

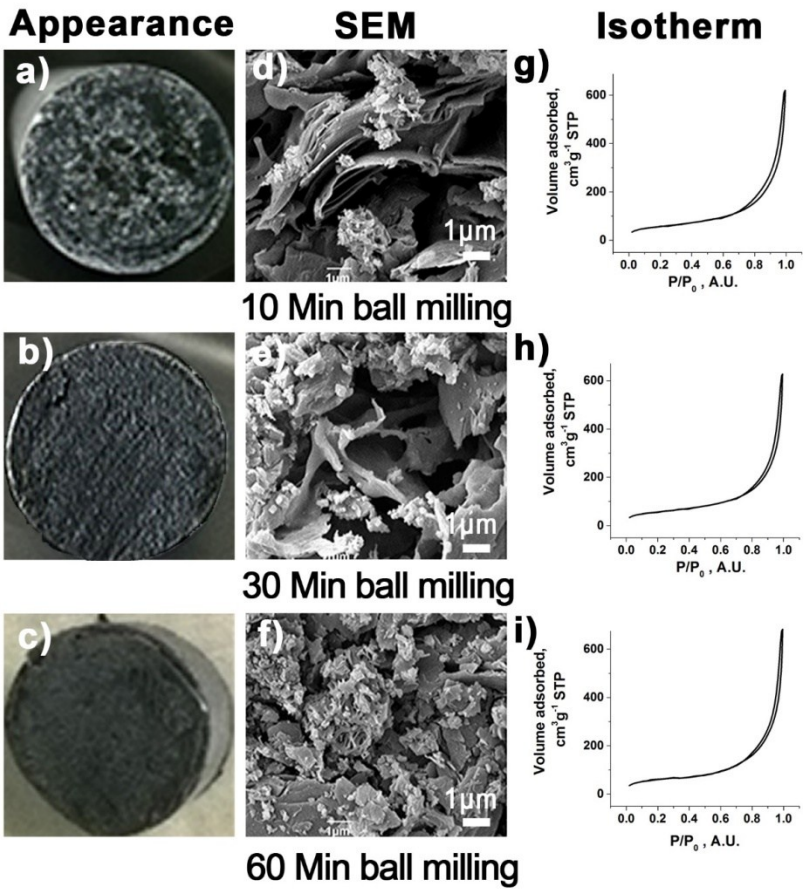

Figure S1. Transversal sections of the mesoporous composite monoliths with 20 % w/w graphite (Starene®140-G20) after a) 10 min, b) 30 min and c) 60 min of ball milling; subfigures d-f show the respective SEM images, and g-i the N_2 adsorption isotherms of the respective samples shown in a-c.

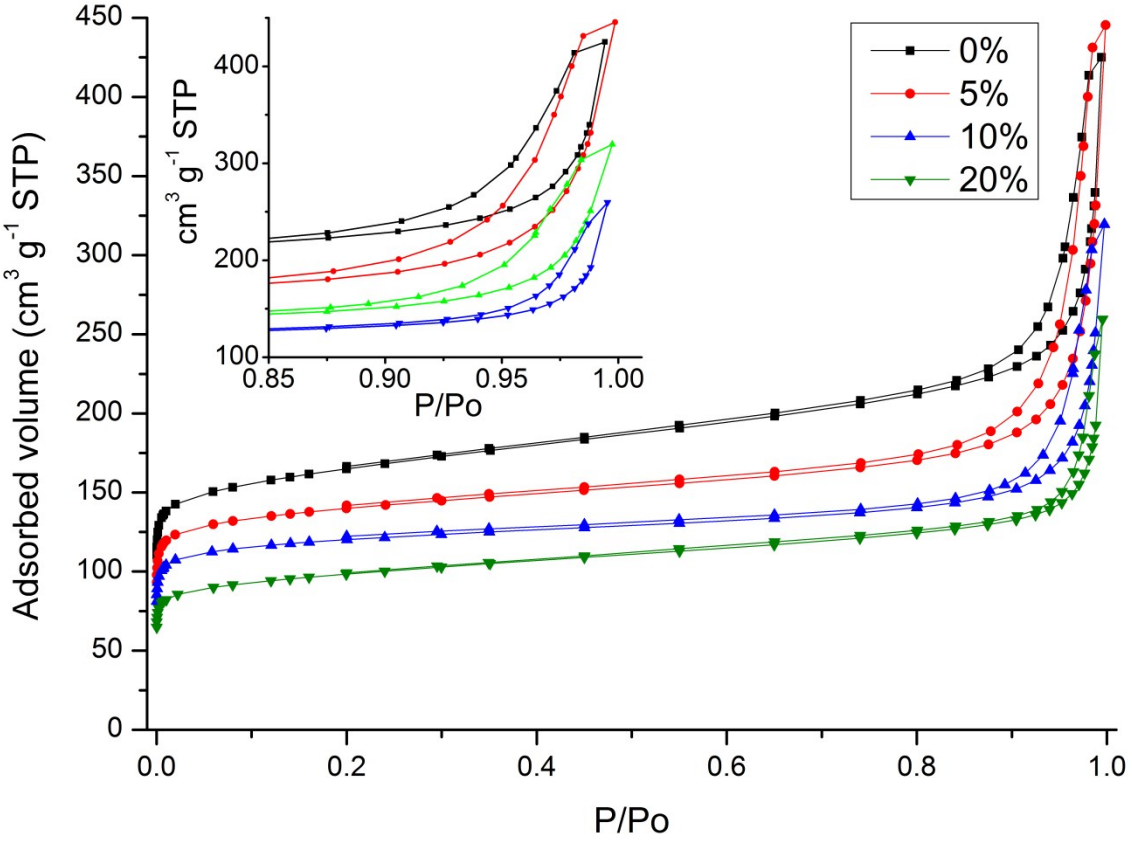

Figure S2. N_2 adsorption isotherms of Starbon®800 and the Starene®800-G5-20 composites. The insert is a zoomed in region of the isotherms hysteresis's, from P/P0 0.85 to 1.0.

Table S1. Textural properties of the prepared composites measured by N_2 adsorption

*BM/ min	Before carbonisation, 20% initial graphite					
	S_{BET} (m^2 g^{-1})	Pore volume (cm^3 g^{-1})	V_{micro} (cm^3 g^{-1})	V_{meso} (cm^3 g^{-1})	[a]Microporosity (%)	[b]Mesoporosity (%)
10	158.8	0.71	0.003	0.707	0.42	99.58
30	158.2	0.75	0.003	0.747	0.40	99.60
60	156.5	0.78	0.003	0.777	0.38	99.62
Graphite/ %	After carbonisation, 800 °C, 30 min ball milling					
	S_{BET} (m^2 g^{-1})	Pore volume (cm^3 g^{-1})	V_{micro} (cm^3 g^{-1})	V_{meso} (cm^3 g^{-1})	[a]Microporosity (%)	[b]Mesoporosity (%)
0	565.1	0.75	0.20	0.43	31.7	68.3
5	475.7	0.69	0.21	0.48	30.4	69.6
10	408.8	0.49	0.19	0.31	38.0	62.0
20	336.7	0.40	0.15	0.26	36.6	63.4

* BM- is ball milling; [a] and [b] calculated from the total of V_{micro} and V_{meso}. using adsorption isotherm.

Table S2. Comparison the Starene® textural properties estimated using different approaches such as the BJH, Dollimore-Heal, DFT and t-plot

Graphite Content	Micropore volume (cm^3g^{-1})			Total pore volume (cm^3g^{-1})					Average pore diameter. Desorption (nm)	
	Dubinin-Astahov	t-plot	DFT	Dollimore-Heal		BJH		DFT	Dollimore-Heal	BJH
				Ads.	Des.	Ads.	Des.			
0%	0.25	0.16	0.16	0.62	0.43	0.75	0.55	0.73	6.7	6.7
5%	0.21	0.15	0.17	0.67	0.48	0.69	0.51	0.48	11.2	11.2
10%	0.19	0.14	0.12	0.48	0.30	0.49	0.33	0.42	11.42	12.1
20%	0.16	0.10	0.12	0.39	0.24	0.40	0.27	0.32	6.8	7.3

Table S3. Conductivity of Starbon®800 and the Starene®800 composites

Initial concentration of graphite (%)	[a]Conductivity ($S \cdot cm^{-1}$)
0	0.0070 ± 0.0005
5	0.0778 ± 0.0021
10	0.1441 ± 0.0095
20	0.1484 ± 0.0017

[a]determination of the error in the conductivity of the samples was carried out by testing them 6 time over 1.5h.

Table S4. XPS elemental analysis of the mesoporous carbons prepared at 800ºC

Element	Original graphite content added (%)			
	0	5	10	20
C	92.7 ± 0.4	96.1 ± 1.1	97.5 ± 0.4	96.5 ± 0.3
O	7.3 ± 0.4	3.9 ± 1.1	2.5 ± 0.4	3.5 ± 0.3

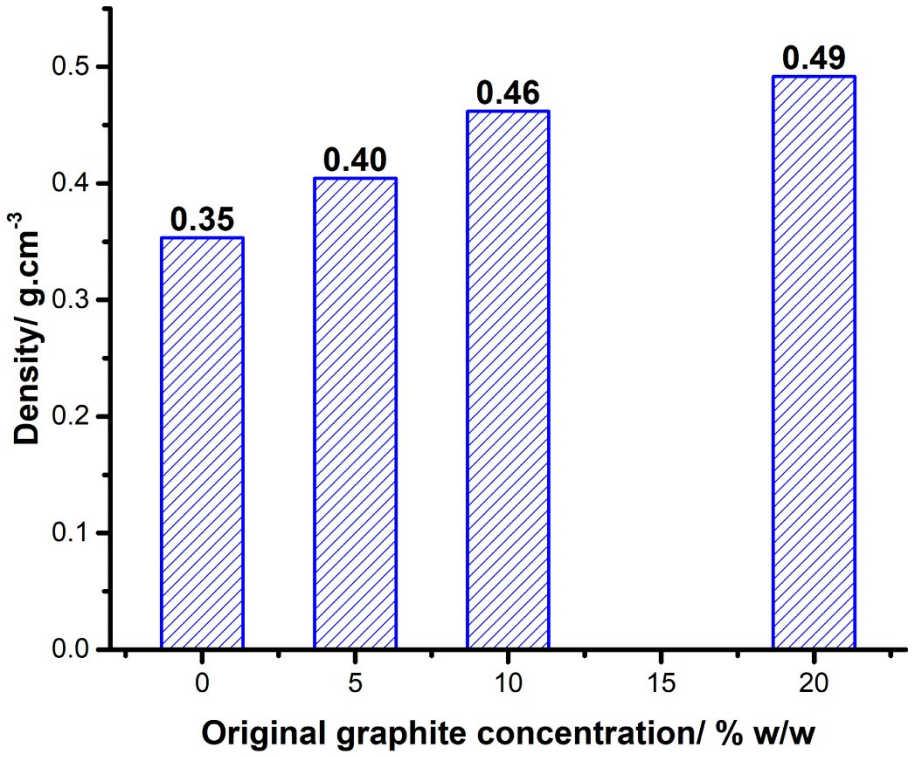

Figure S3. Influence of original graphite concentration on the density of the final composite materials obtained at 800°C (Starene®800-G0-20).

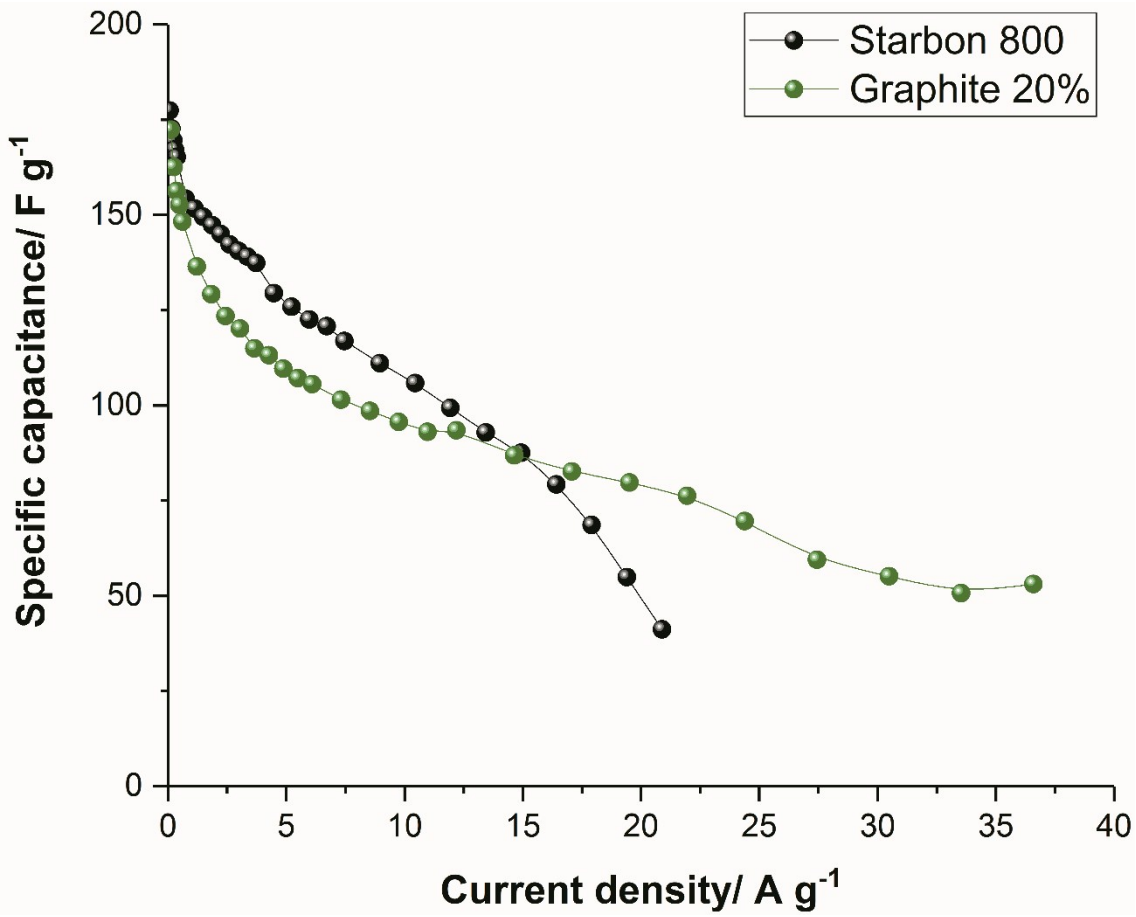

Figure S4. Rate capability of Starbon 800 (0% w/w graphite) and the Starene material with 20% w/w graphite.

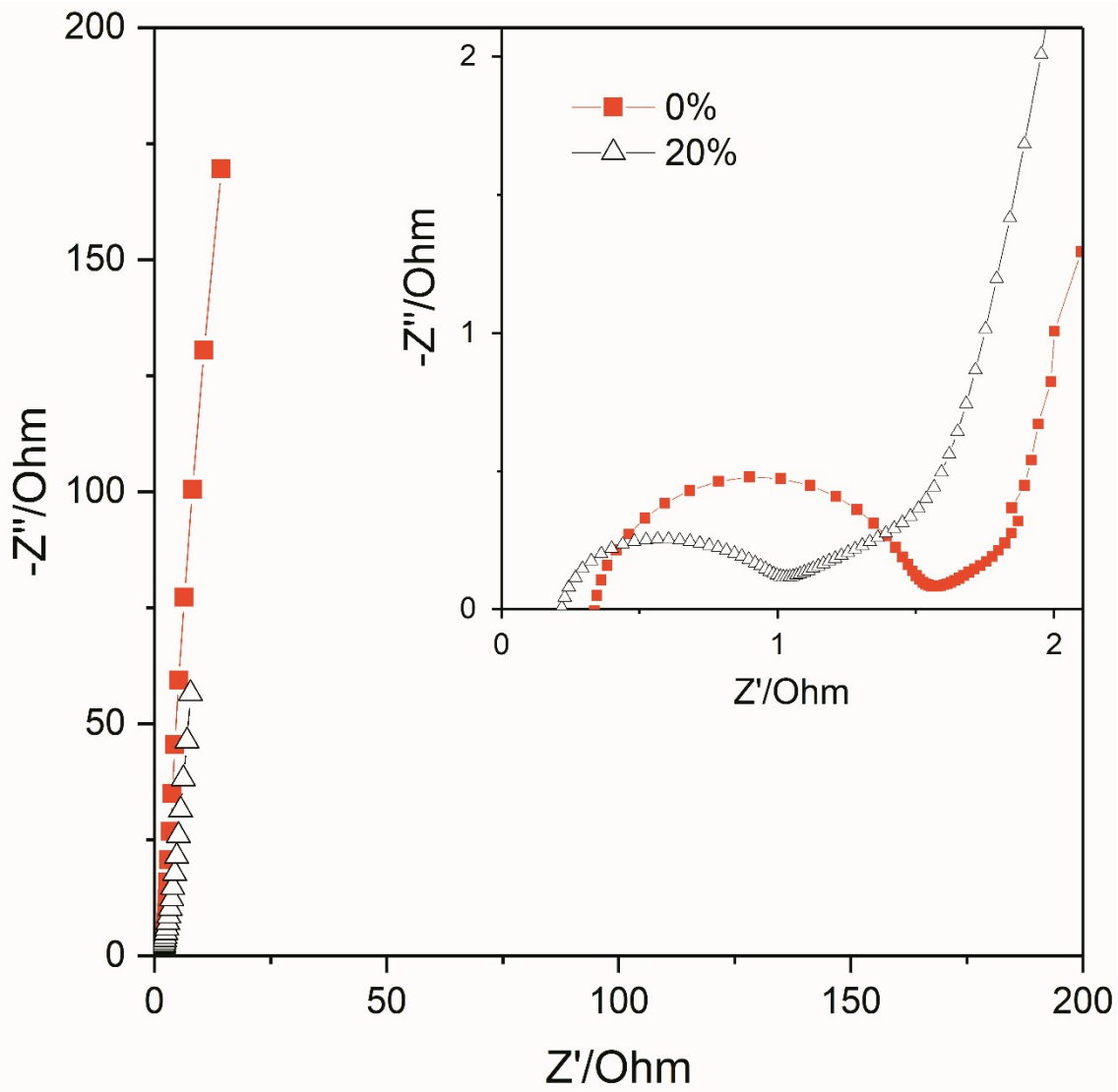

Figure S5. Nyquist plot of Starbon® (red) and the Starene® composite prepared with 20% w/w graphite, and the insert of the same plot but only containing the high frequency region.

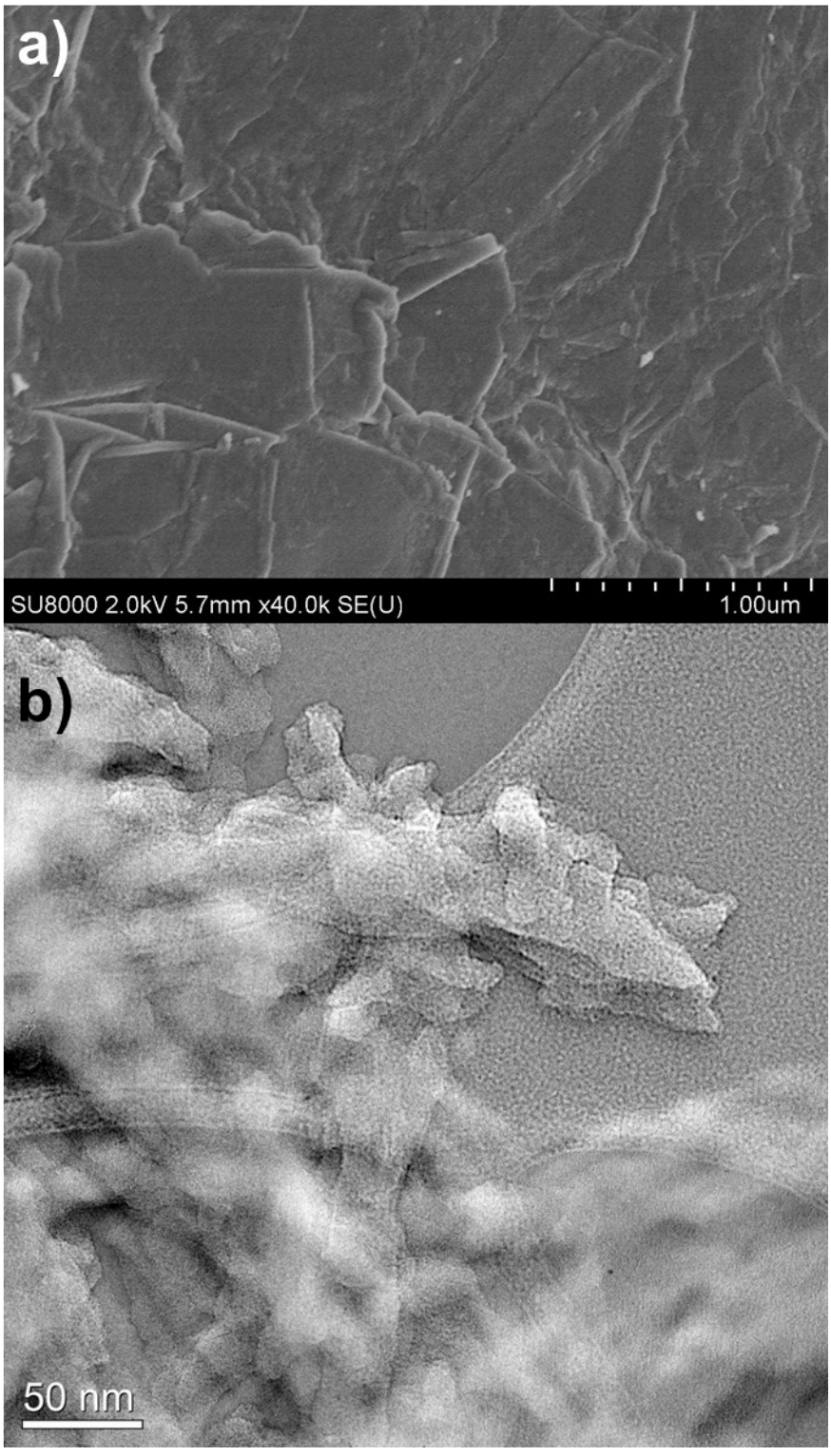

Figure S6. a). SEM image of the starch-graphite composite ball-milled mixture before gelatinisation (see Figure S1 for after gelatinisation); b). TEM image of the Starene®800-G20.

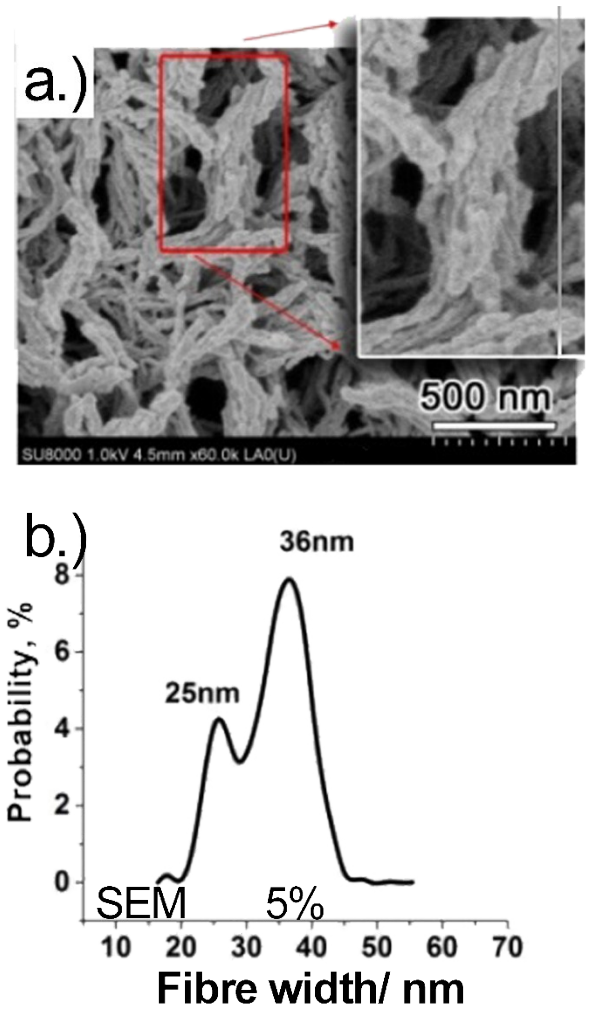

Figure S7. a). HRes SEM images of the mesoporous carbons prepared at 800ºC with 5% w/w graphite, and b) is the particle size distributions derived from the image shown in a).

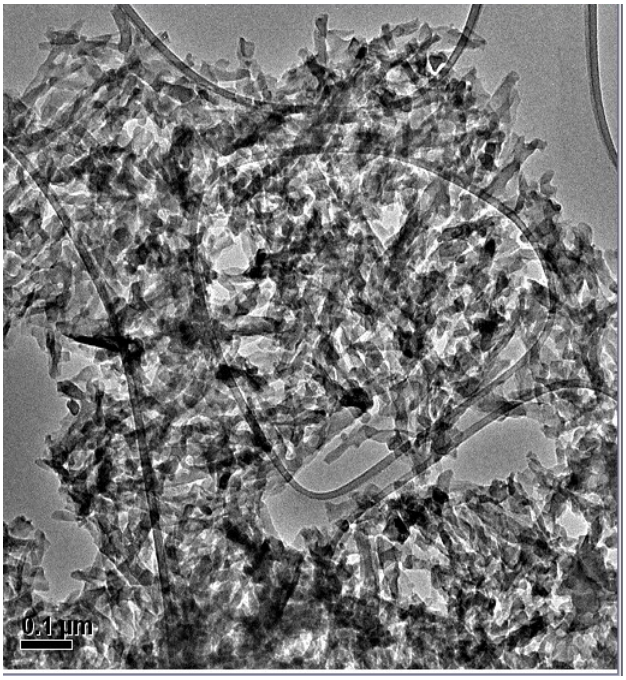

Figure S8. TEM of Starene®800_20%, magnification 5.13 K

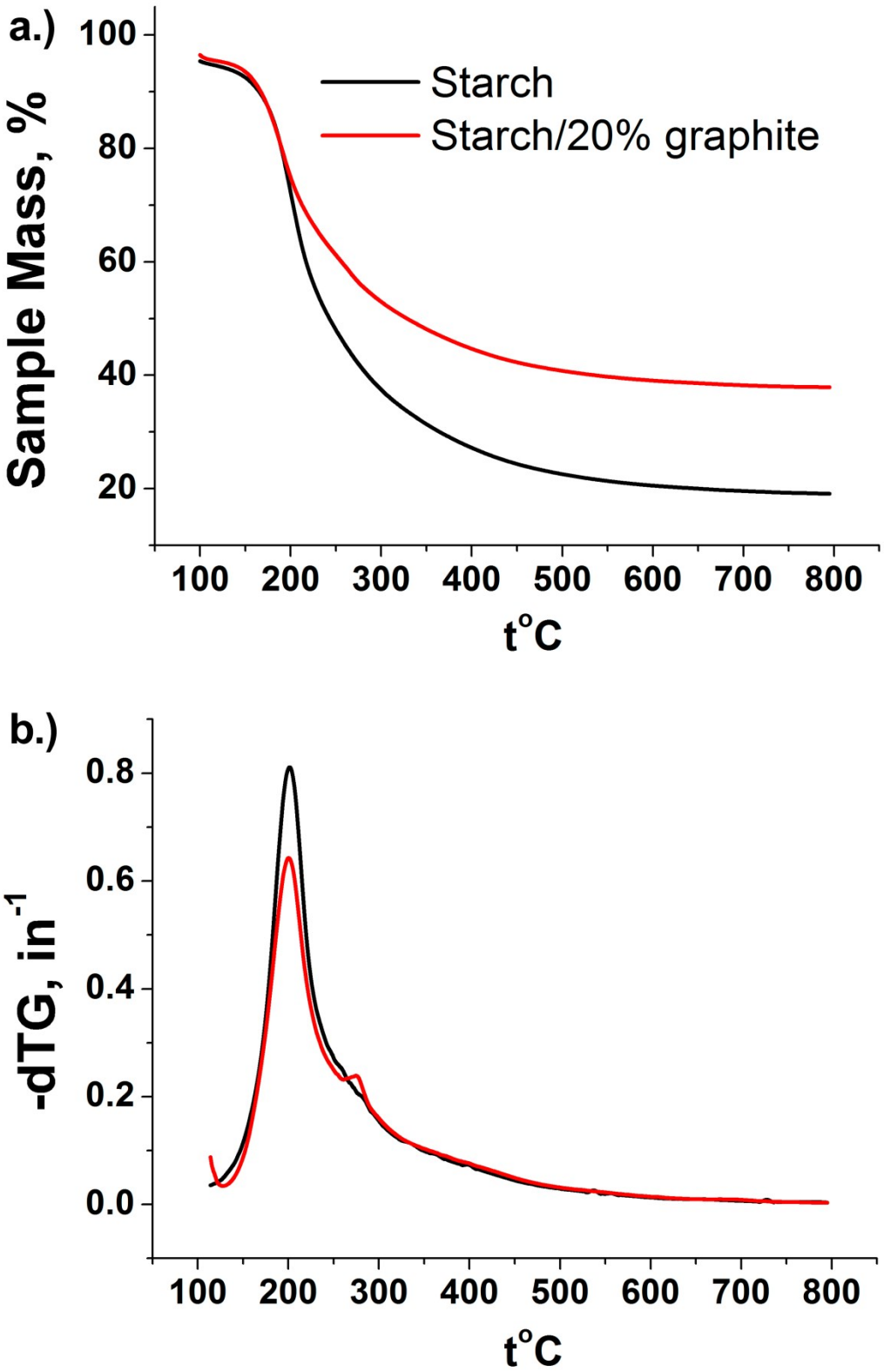

Figure S9. a.) TGA traces of a mesoporous starch monolith and a composite mesoporous starch monolith containing 20%w/w graphite, both doped with 5%w/w pTSA and heated at 1ºC/minute under a nitrogen atmosphere, and b.) there respective dTG traces.

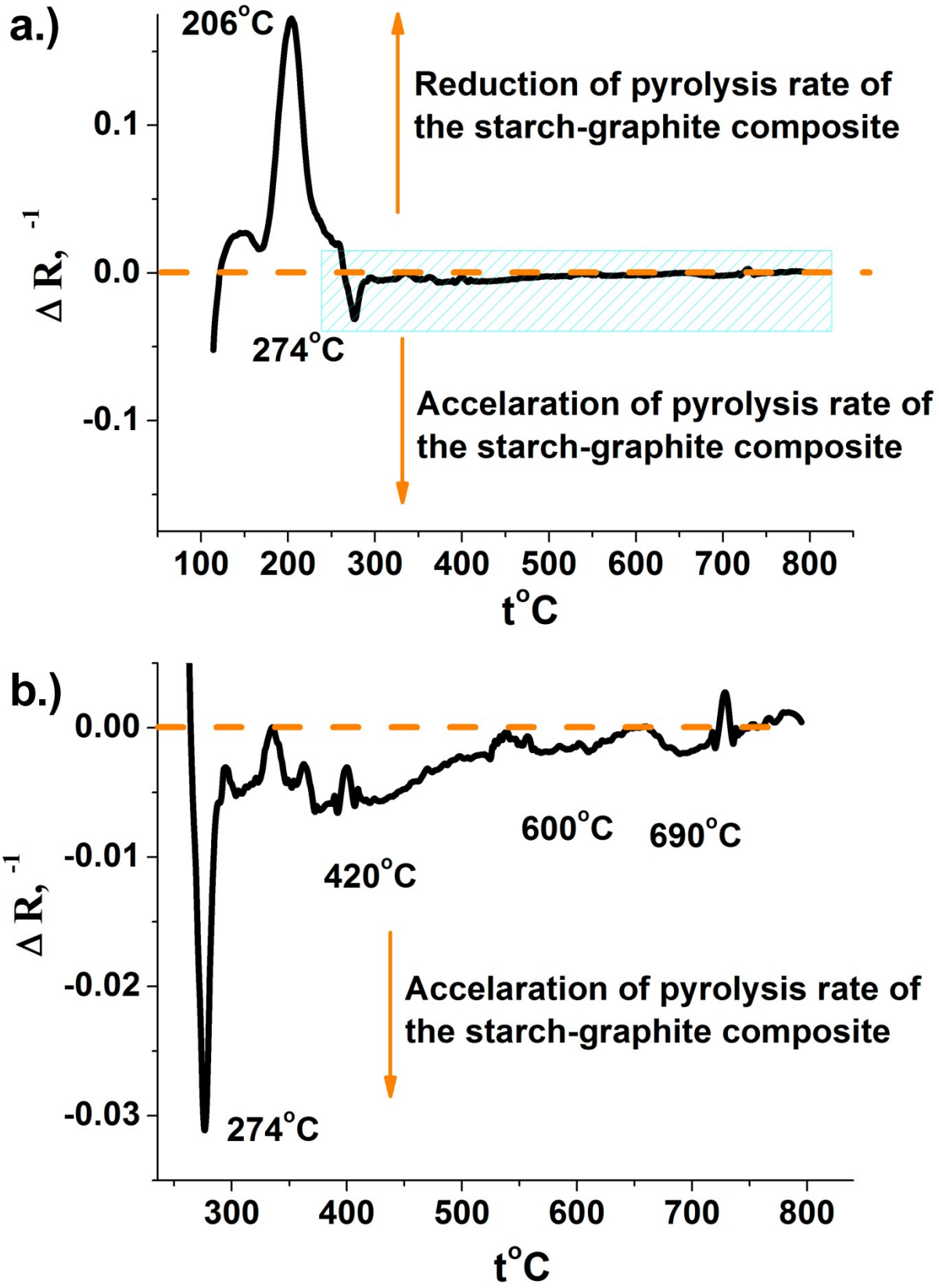

Figure S10. a.) TGA data (Figure Sx1a) of the 20%w/w graphite composite normalized to its starch content, and then subtracted from the dTG trace of the pure starch, and b.) zoomed in region between 250 and 800ºC of the trace shown in a.).

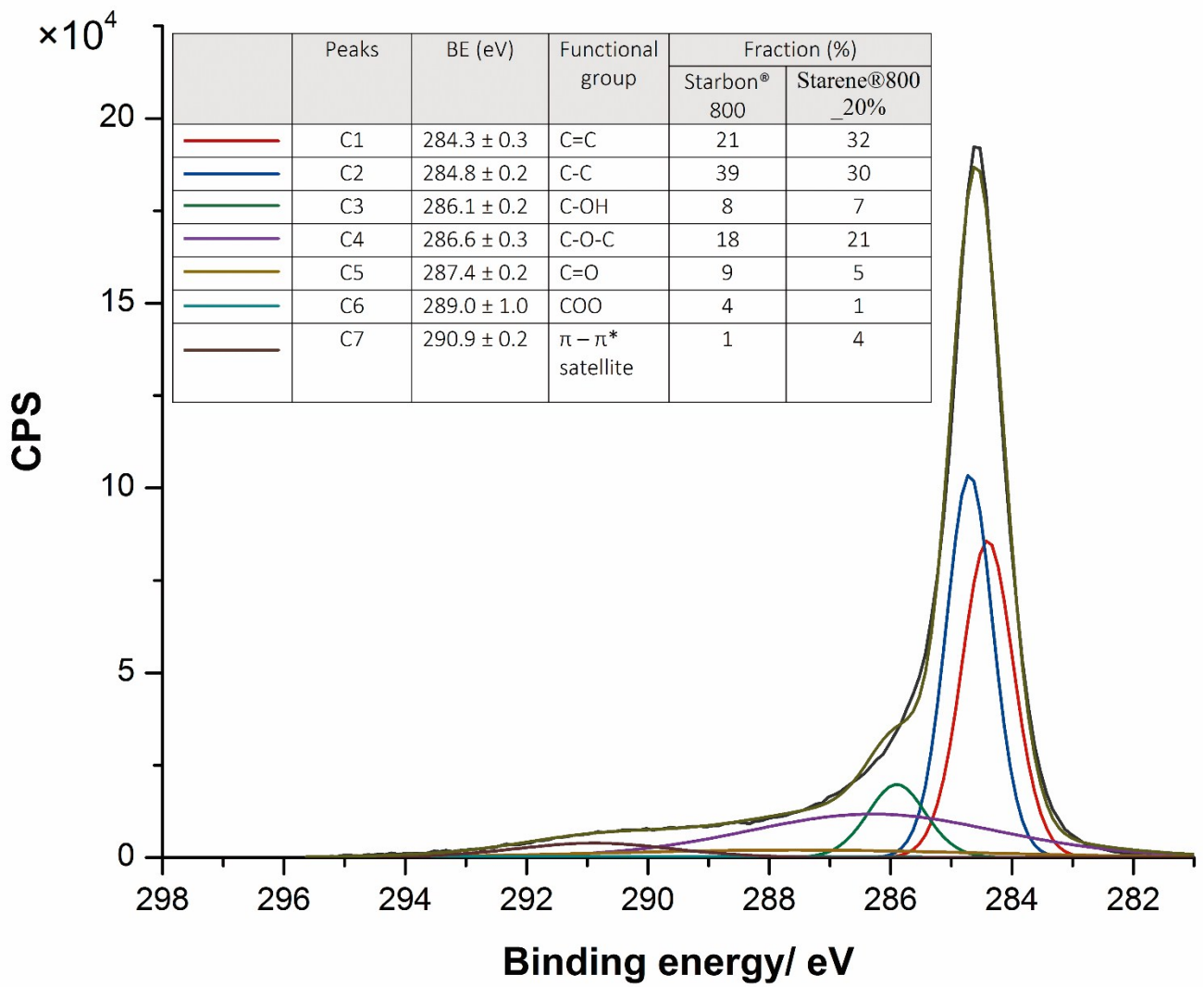

	Peaks	BE (eV)	Functional group	Fraction (%)	
				Starbon® 800	Starene®800 _20%
	C1	284.3 ± 0.3	C=C	21	32
	C2	284.8 ± 0.2	C-C	39	30
	C3	286.1 ± 0.2	C-OH	8	7
	C4	286.6 ± 0.3	C-O-C	18	21
	C5	287.4 ± 0.2	C=O	9	5
	C6	289.0 ± 1.0	COO	4	1
	C7	290.9 ± 0.2	π – π* satellite	1	4

Figure S11. High-resolution XPS spectra in the C1s BE region of Starene®800_20%.

Table S5. Crystallinity parameters of the mesoporous carbons prepared at 800ºC, calculated from XRD analysis.

Sample	Peak	FWHM	La (nm)	Lattice strain	d-spacing (nm)	G layers
Grafito	26.63	0.1900	44.91	0.0035	0.3345	134
G-Starch BM 20%	26.66	0.2575	33.13	0.0047	0.3340	99
G-Starch BM 20% (heated to 800 ºC)	26.50	0.3156	27.02	0.0058	0.3361	80
*Starbon800	25.16	8.1993	1.04	0.1603	0.3537	(2.9)
Starene 800-G5	26.41	0.4064	20.98	0.0076	0.3372	62
Starene 800-G10	26.48	0.3526	24.18	0.0065	0.3363	72
Starene 800-G20	26.49	0.3163	26.96	0.0059	0.3362	74

* Note/ the Starbon 800 sample is a turbostratic mesoporous carbon, with the value included for comparison.

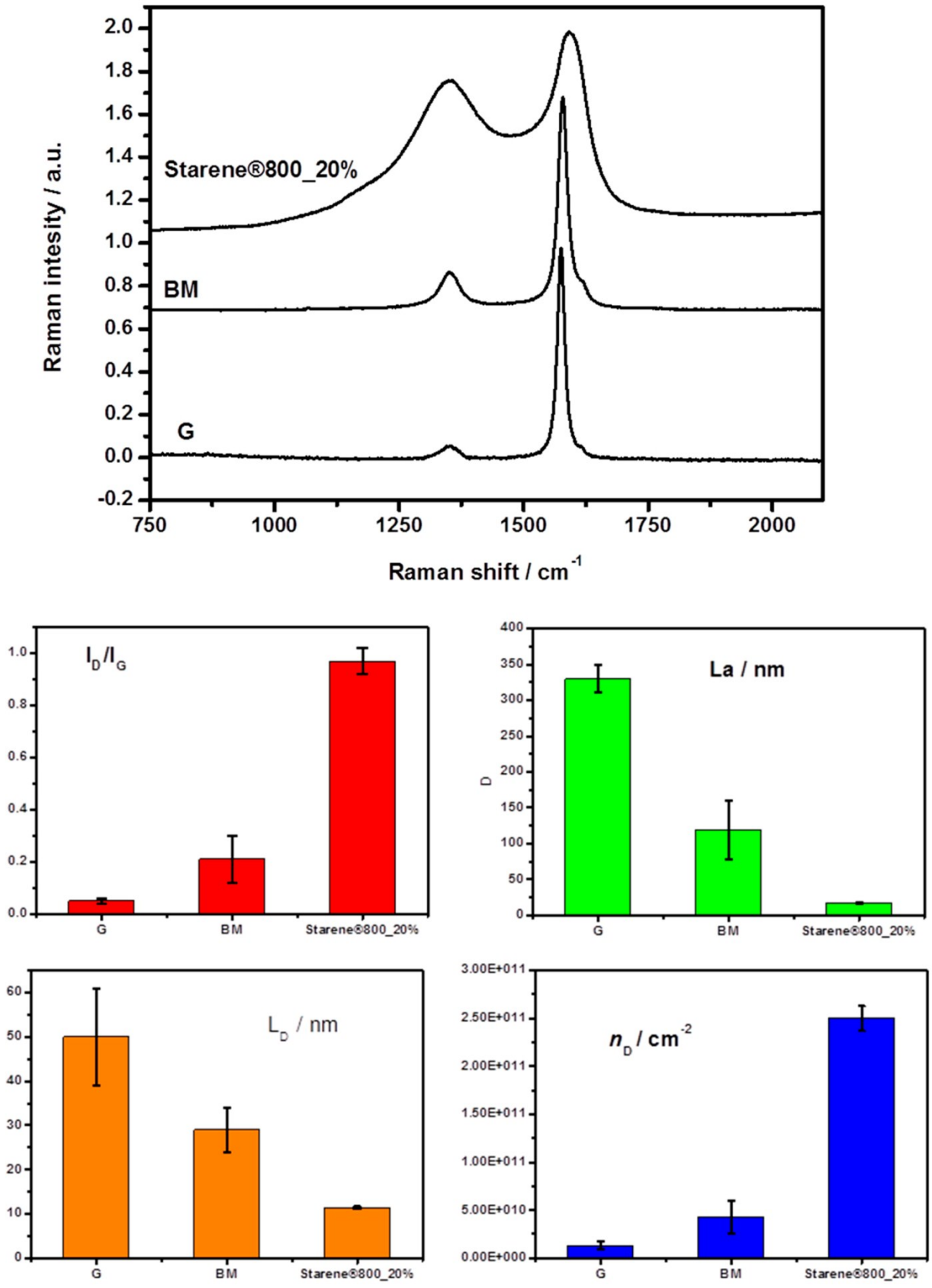

Figure S12. Raman spectra of graphite, graphite after ball milling and Starene®800_20%. Graphs of I_D/I_G, La, L_D and n_D showing the impact of processing on the graphite structure.

The main features shown in the Raman spectra of the carbon materials are the primary E_{2g} in-plane vibration mode (G band) appearing at 1576, 1579 and 1592 cm^{-1} and the disorder-induced D band at 1359, 1352 and 1352 cm^{-1} for the graphite, graphite after ball milling and the Starene®800_20% samples respectively. The A_D/A_G ratios for these materials changes from 0.10 ± 0.03 for the graphite before processing to 0.35 ± 0.09 after ball milling to 2.05 ± 0.29 for the Starene®800_20% sample. For the latter, the much higher A_D/A_G ratio as well as the broader bands are related to the contribution from the amorphous carbon after pyrolysis. However, the spectra of samples before and after the ball-milling are similar, with sharp D and G contributions, with the only difference being a shoulder centred at 1620 cm^{-1}, the D' band originating from edge defects in the graphitic material.[1] This is more prominent in the material after ball milling as the graphite sheets have being broken down into a smaller size.

Calculation of the mean in-plane crystallite size,[2] L_a from analysis of the I_D/I_G ratio (intensity) of the samples shows that the size decreases significantly from 330 ± 19 to 119 ± 41 and 17 ± 1 for graphite before and after ball milling, and after carbonisation within the porous matrix (Starene®800_20%) respectively. Measurement of the density of defects, n_D another parameter in which to analyse the quality of materials shows again that there is a tendency of increasing the amount of defects in the graphite, from $1.3 \times 10^{10} \pm 3.8 \times 10^{9}$ to $4.3 \times 10^{10} \pm 1.7 \times 10^{10}$ and $2.5 \times 10^{11} \pm 1.3 \times 10^{10}$ defects per cm^2 for the ball milled graphite and nanocomposite respectively. The distance between the defects also decreases with processing with ball milling reducing the value by about 40% to 29 ± 5 nm from 50 ± 11 and a further 60% to 11.4 ± 0.3 for the nanocomposite, again showing the effect heating and contact with the carbonized starch is having on the graphite particles.

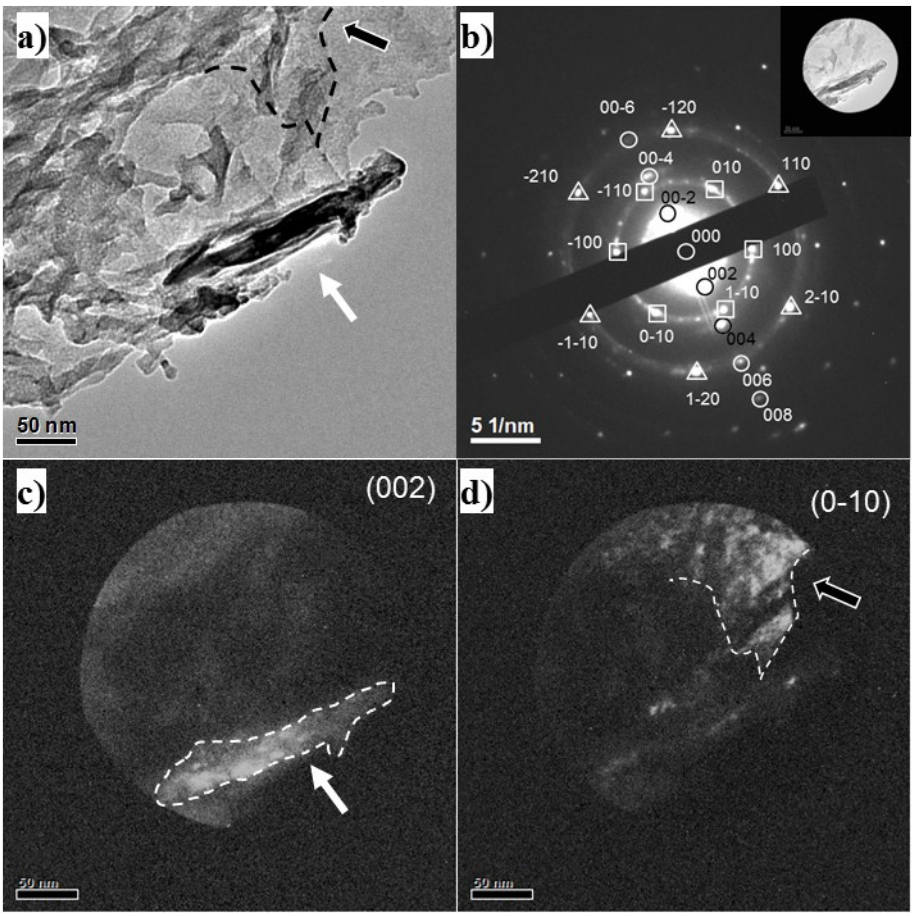

Figure S13. a) Bright field TEM image of the porous carbonaceous material with graphite (5%), showing a region that includes graphitic flakes. b) Selected area electron diffraction pattern from the area of the sample shown in the inset. Circles mark the 002 Bragg spot sequence from the stacking planes along the C-axis of graphite. Squares and triangles mark the in-plane diffraction spots of the (010), (110) and (2-10) type.

Significant crystallinity can be observed in the composite as derived from the electron diffraction patterns as shown in Figure S13b. The Bragg spots were obtained from the region defined by the selected area aperture in the inset of Figure S13b. Circled diffraction spots Figure S13b correspond to (002) atomic planes of graphite with atomic plane distance of 0.335 nm. Dark field imaging, by using the (002) diffraction spot (Figure S13c), shows the graphitic region of the specimen oriented along the c-plane (001) perpendicular to the electron beam. Squares and triangles in Figure S13b mark the in-plane (010)-type and (110)-type reflection spots from a graphite flake imaged along the c-axis (001). Similarly, Figure 13d is a dark field image obtained using the (0-10) spot. A dashed white line contour reveals the diffracting flake responsible for the in-plane Bragg spots in the

diffraction pattern. The same flake can be seen in Figures S13a indicated by the black arrow and the black dashed line contour.

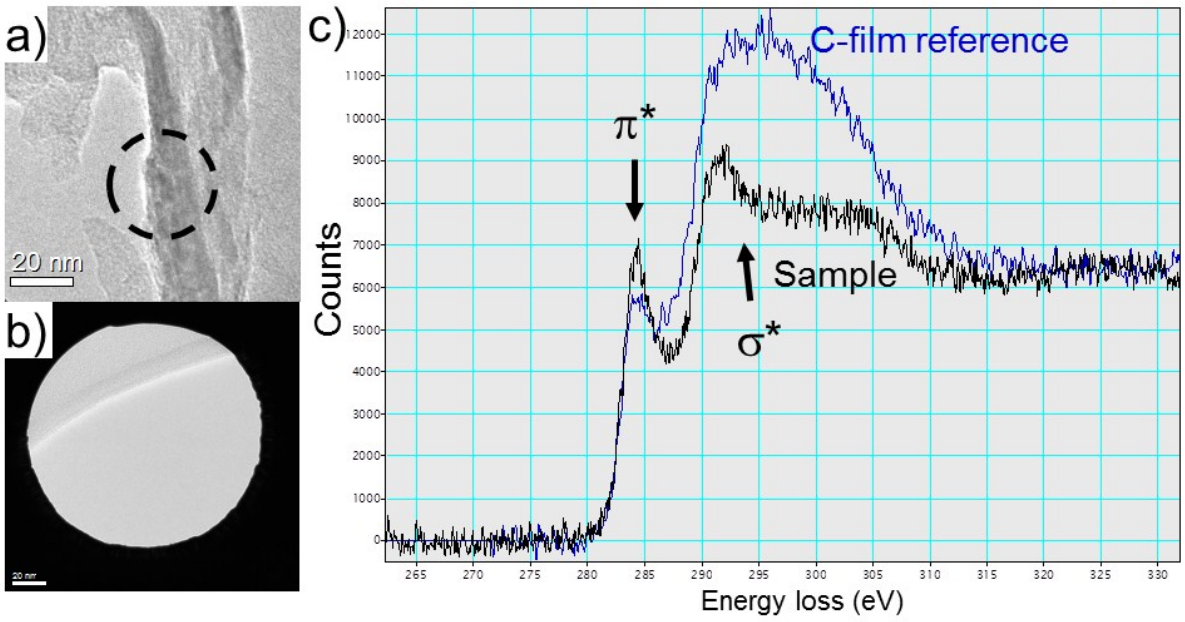

Figure S 14. a) TEM image showing an area containing graphitic flakes, the blak dashed circle indicates the area selected to collect the EELS sample spectrum in c); b) area of the amorphous carbon film used to collect the reference spectrum in c, and; c) background subtracted C-K edges from the areas in a) and b).

The fingerprint of the graphitic nature of the flakes (π* and σ* peaks), was investigated using EELS. The Carbon-K edges fine structure from the area indicated by the dashed circle, **Figure S14a** where a single flake can be observed, is shown in **Figure S14c**. An EELS spectrum was acquired from the amorphous C film for comparison, **Figure S14b**. The π* and σ* peaks from the C molecular orbitals characteristic for graphitic flakes are clearly observed in comparison to amorphous C K-edge. Both EELS spectra and diffraction studies show that the materials processing does not alter the crystalline nature of the graphite at the nanoscale.

1. A. C. Ferrari, *Solid State Communications*, 2007, **143**, 47-57.
2. L. G. Cançado, K. Takai, T. Enoki, M. Endo, Y. A. Kim, H. Mizusaki, A. Jorio, L. N. Coelho, R. Magalhães-Paniago and M. A. Pimenta, *Applied Physics Letters*, 2006, **88**, 163106.